



Luminescent cationic/neutral Cu(I) complexes for use in light-emitting diodes: Synthesis, structural characterization, DFT studies and properties

Ting-Hong Huang^{a,b,*}, Cheng Luo^b, Dan Zheng^b

^a School of Materials and Energy, University of Electronic Science and Technology of China, Chengdu, 611731, China

^b School of Chemical Engineering, Sichuan University of Science & Engineering, Zigong, 643000, China

ARTICLE INFO

Keywords:

Cationic and neutral Cu(I) complexes
Crystal structures
Luminescent properties
Temperature
Light-emitting diodes

ABSTRACT

Cationic and neutral mononuclear Cu(I) complexes, [Cu(PPh₃)₂(PmH)]BF₄ (1a), [Cu(DPEphos) (PmH)]BF₄ (2a), [Cu(Xantphos) (PmH)]BF₄ (3a), [Cu(PPh₃)₂(Pm)] (1b), [Cu(DPEphos) (Pm)] (2b) and [Cu(Xantphos) (Pm)] (3b) (PPh₃ = triphenylphosphine, DPEphos = bis(2-diphenylphosphinophenyl)ether, Xantphos = 9, 9-dimethyl-bis(diphenylphosphino)xanthenes, PmH = 2-(pyridin-2-yl)benzimidazole, Pm = (2-(Pyridin-2-yl)benzimidazolato), have been prepared and characterized by IR, ¹H NMR, ¹³C NMR, ³¹P NMR, XRD, elemental analysis and X-ray crystal structure analysis. The structural analysis shows that each of Cu(I) complexes includes a tetrahedral [Cu(NN)(PP)]⁺ moiety, and temperature variation from 99 K to 298 K leads to the change of bonds lengths, angles and weak interactions. Meanwhile, theoretical calculations indicate that the differences between cationic and neutral Cu(I) complexes affect the composition of HOMO and LUMO orbitals, and the effect of temperature on Mulliken atomic charges is limited. Furthermore, neutral Cu(I) complexes 1b–3b show better luminescence in comparison to cationic Cu(I) complexes 1a–3a at room temperature, and temperature variations from 99 K to 298 K result in changing photoluminescence to some extent, which partly agrees with the related calculation results. In these cationic and neutral Cu(I) complexes, the maximum phosphorescent lifetime and quantum yield reach respectively 137 μs and 42% at room temperature. Moreover, cationic and neutral Cu(I) complexes are utilized to fabricate the monochromatic LEDs, showing favorable electroluminescence with the maximum EQE of 7.10%.

1. Introduction

Photoluminescent metal complexes continue to attract attention due to their practical applications in chemical probes, chemosensors, biological imaging, photochemical catalysts, light-emitting diodes (LEDs) and dye-sensitized solar cells (DSSCs) [1–8]. Therefore, on the basis of transition metal, it is particularly important to design and synthesize highly-efficient luminescent complexes. Nowadays, metal copper have been reported as an important candidate for synthetic copper(I) complexes with high-efficiency luminescence [9–12], because metal copper is more abundant than other luminescent materials like Ru and Pt [13, 14]. Meanwhile, a large amount of copper(I) complexes based on the different kinds of ligands, such as N-ligands, P-ligands and N, P-ligands, are prepared and used for solid-state lighting technologies like LEDs [15–17]. Furthermore, the studies of luminescent properties show that many factors affect photoluminescence of copper(I) complexes, i.e. ligand types, weak interactions, solvent and the form of complexes

[18–22]. For example, Hou and co-workers reported that a series of new functional phosphine ligands with different central arene spacers (phenyl, naphthyl, biphenyl) are used to construct highly-effective, binuclear copper(I) complexes [23]; Shi and co-workers reported that neutral [Cu(nimp)(PP)] complexes show better luminescence in comparison with ionic [Cu(nimpH)(PP)]PF₆ complexes [24]; Xin and co-workers presented that, owing to the restriction of intramolecular rotation, copper(I) complexes display aggregation-induced phosphorescence emission behavior in CH₂Cl₂/hexane [25]; Gernert and co-workers demonstrated that the expanded π-system of the CAARc results in the formation of unusually deep red emitting Cu(I) complexes with thermally activated delayed fluorescence (TADF) [26]. These work show that the luminescent properties of copper(I) complexes can be improved by tuning relative influence factors. That is to say, the variation of multiple factors may be a convenient way of mediating luminescent properties.

Temperature variation has been used to tune structures and

* Corresponding author. University of Electronic Science and Technology of China, Chengdu, 611731, China.

E-mail address: hth_chem@126.com (T.-H. Huang).

<https://doi.org/10.1016/j.orgel.2021.106273>

Received 3 April 2021; Received in revised form 20 June 2021; Accepted 20 June 2021

Available online 1 July 2021

1566-1199/© 2021 Published by Elsevier B.V.

luminescent properties of copper(I) complexes [27–30]. For example, the solid-state emission of a copper(I) complex, [Cu(POP) (Me-DPSO)] [BF₄], ranges from orange at room temperature to yellow at low temperatures [31]. Meanwhile, temperature-dependent crystal structures and luminescence are presented by Moussa and co-workers [32]. These studies show that temperature has an important influence on constructing the highly-efficient, luminescent copper(I) complexes. However, at present, temperature effect has rarely been incorporated into theoretical calculation of copper(I) complexes [33]. Therefore, the development of theoretical calculation at different temperatures is important for observing the effect of temperature, which is in favor of investigating the relationship between structure and luminescent properties and then obtaining highly luminescent copper(I) complexes.

Consequently, cationic and neutral Cu(I) complexes, [Cu(PPh₃)₂(PmH)]BF₄ (1a), [Cu(DPEphos) (PmH)]BF₄ (2a), [Cu(Xantphos) (PmH)]BF₄ (3a), [Cu(PPh₃)₂(Pm)] (1b), [Cu(DPEphos) (Pm)] (2b) and [Cu(Xantphos) (Pm)] (3b), have been constructed and characterized. Meanwhile, the structures, theoretical calculation and luminescent properties of these cationic and neutral Cu(I) complexes are investigated, which aims to observing the influence of the form of copper(I) complexes on structure and luminescent properties. Furthermore, take the case of complex 1b, the single crystal X-ray diffraction data for this copper(I) complex are collected at 99 K, 150 K, 200 K, 250 K and 298 K, and then the related theoretical calculation and luminescent properties of copper(I) complexes at different temperatures are studied to consider effect of temperature. Moreover, the monochromatic LEDs using copper (I) complexes as emitting materials demonstrate fairly good electroluminescence (EQE_{max} = 7.10%).

2. Result and discussion

2.1. Syntheses

Cationic Cu(I) complexes 1a-3a are formed by the reaction of copper (I) salt with phosphine ligands and PmH in a ratio of 1:2:1 or 1:1:1. And these cationic complexes reacting with excessive KOH would produce neutral Cu(I) complexes 1b-3b. In these six Cu(I) compounds, the IR peaks of 1434–1437 cm⁻¹ and 1588–1601 cm⁻¹ are assigned to $\nu_{\text{P-H}}$ and $\nu_{\text{C=N}}$, respectively, reflecting the presence of the binding patterns of phosphine ligands (PPh₃, DPEphos and Xantphos) and imidazole ligands (PmH or Pm). Similarly, ¹H and ¹³C spectra show anticipated resonances typical for the coordinated ligands of these six Cu(I) complexes (Figs. S1–S6). Meanwhile, the ³¹P NMR peaks of cationic and neutral Cu (I) complexes are quite different, indicating different phosphorus and

electronic environments (Figs. S7–S12). Moreover, the experimental powder XRD patterns of cationic and neutral Cu(I) complexes are almost identical with simulated profiles, only being a bit difference on detail, which may be due to the solid samples including solvent molecules (Fig. 1, S13 and S14).

2.2. Structure analysis

The structure of complex 1a is analogue to the previously reported (Fig. S15) [34]. Therefore, only the structures of 2a, 3a and 1b-3b are demonstrated here on detail. The single crystal X-ray diffraction analysis shows that both 2a and 3a contain one [Cu(NN) (PP)]⁺ moiety, which adopts a distorted tetrahedral geometry constructed by two N atom from PmH and two P atoms from phosphine ligands (Fig. 2). In these two complexes, the Cu–N and Cu–P bond lengths are in the range of 2.076 (5)–2.129(4) Å and 2.2429(19)–2.2710(18) Å (Table S3), respectively, which are close to those in previously studied [Cu(NN) (PP)]⁺ system, such as [Cu(PPh₃)₂ (DPA)]BF₄ [35] and [Cu(DPEphos) (DPSO₂)] [BF₄] [36]. Corresponding N–Cu–N, N–Cu–P and P–Cu–P bond angles are 79.78(17)–80.1(2)°, 110.85(15)–116.77(15)° and 115.31(5)–115.64(7)° (Table S3), respectively, which are similar with previously reported [Cu (NN) (PP)]⁺ species, e.g. [Cu(dmp) (dfppe)]PF₆ [37]. Meanwhile, Intra- and inter-molecular $\pi \cdots \pi$ interactions in three complexes are observed with the ring-central distances of 3.96–3.98 Å and dihedral angles of 21.47–22.99° [38], while C–H $\cdots \pi$ interactions are found, with CH/ π distances of 2.63–2.95 Å and angles of 139–178° [39]. Moreover, C–H \cdots F and N–H \cdots F hydrogen bonds are also involved in three complexes (C–H \cdots F hydrogen bonds: H \cdots F = 2.42–2.54 Å, C \cdots F = 3.26–3.39 Å; N–H \cdots F hydrogen bonds: H \cdots F = 1.95–2.01 Å; N \cdots F = 2.76–2.82 Å).

For 1b-3b, the overall structures are similar with that of complexes 1a-3a. However, different from 1a-3a, complexes 1b-3b are neutral four-coordinated by two N atom from Pm and two P atoms from phosphine ligands (Fig. 3 and Fig. 4). The Cu–N and Cu–P bond lengths in 1b-3b are 2.008(2)–2.154(4) Å and 2.2393(11)–2.2987(14) Å (Table 1 and Table S3), respectively, which are analogous to previously investigated copper(I) complexes containing imidazole ligands. Corresponding N–Cu–N, N–Cu–P and P–Cu–P bond angles are 80.08(13)–80.99(9)°, 105.23(8)–122.62(12)° and 111.80(5)–119.63(3)° (Table 1 and Table S3), separately, which are comparable with those of [POP-CuPhPt] [40] and [Cu(DPEphos) (NPh₂)] [41]. Similarly, complexes 1b-3b contain C–H $\cdots \pi$ interactions, with CH/ π distances of 2.50–2.99 Å and angles of 119–155°. Meanwhile, only $\pi \cdots \pi$ interactions of 1b and 2b are found, with the ring-central distances of 3.69–3.99 Å and dihedral

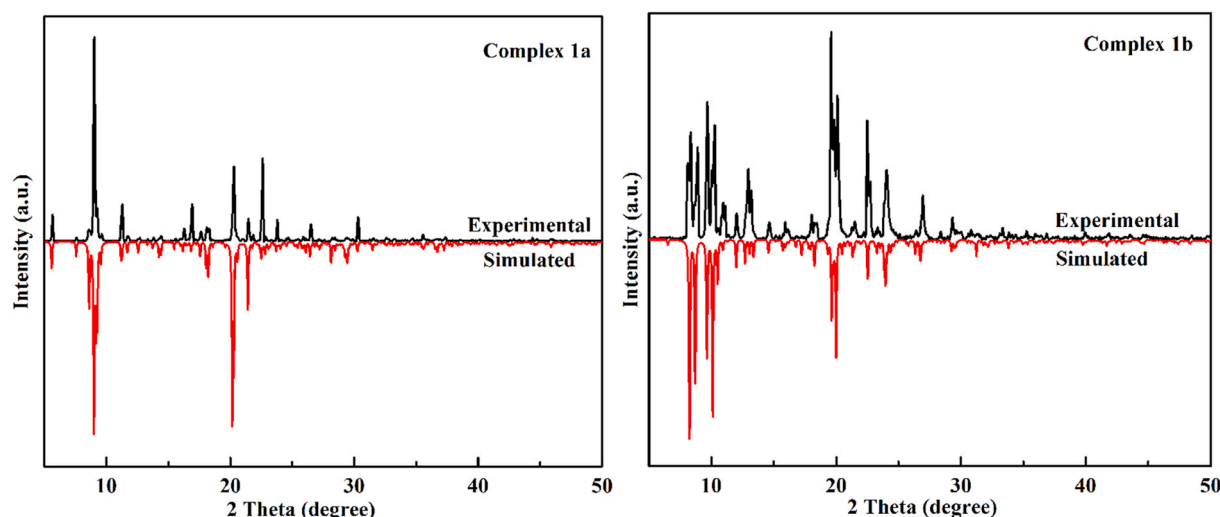


Fig. 1. XRD patterns of compounds 1a (left) and 1b (right) observed by simulation and experiments.

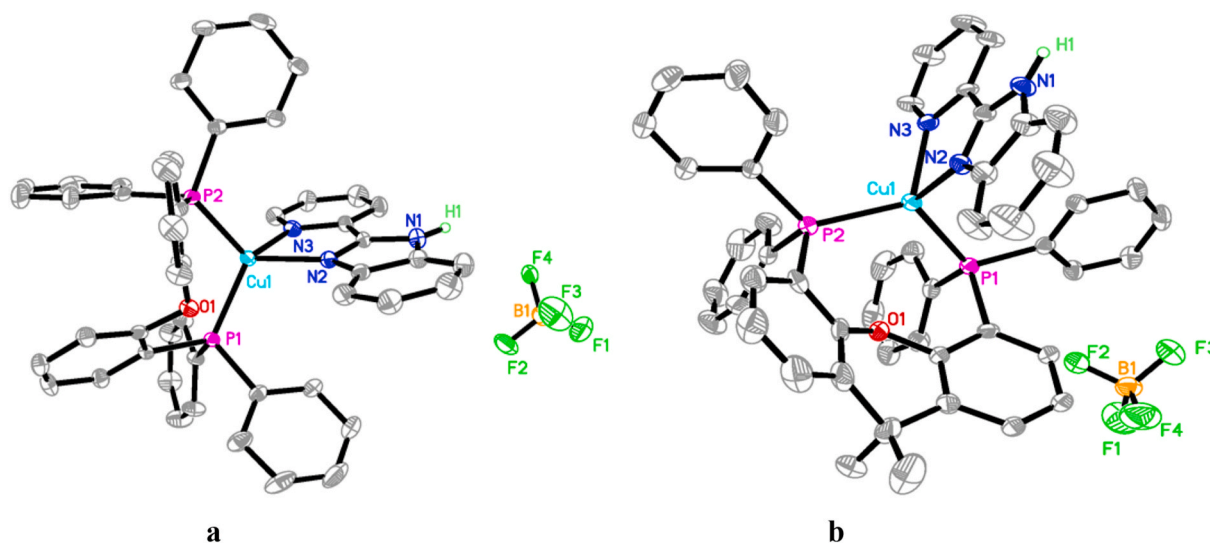


Fig. 2. Molecular structures of 2a (a) and 3a (b). Except for H1, the hydrogens are deleted for clarity.

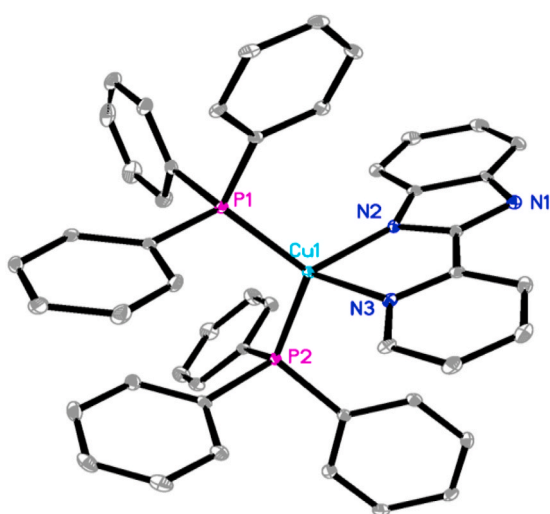


Fig. 3. Molecular structures of 1b. The hydrogens are deleted for clarity.

angles of 0–16.58°.

To observe the effect of temperature on bond lengths and angles, the single crystal structure data of complexes 1b are collected at 99 K, 150 K, 200 K, 250 K and 298 K. As presented in Table 1, temperature variation has a certain degree influence on bond lengths and angles: (1) with the rise of temperature, the Cu–N and Cu–P bond distances will have a little change; (2) at 99–298 K, corresponding P–Cu–P bond angles are largened by 0.89°, while N–Cu–N and N–Cu–P bond angles have a slight variance. As previously reported [42,43], the P–Cu–P bite angle has a major impact on the orbital overlap integral between the occupied $d\pi$ -orbitals from the central copper(I) and the P-localized lone-pairs from the P ligand, which can affect MLCT transitions. Therefore, temperature variation, which is useful to modify bond lengths and angles, may an appropriate method for tuning structures and luminescent properties. Meanwhile, the mean interplanar separation between two pyridyl rings from two neighboring $[\text{Cu}(\text{PPh}_3)_2(\text{Pm})]$ molecules ranges from 3.691 Å to 3.731 Å at 99–298 K (Fig. S16), implying that intermolecular $\pi \cdots \pi$ interactions will change with increasing temperature. Corresponding intra- and inter-molecular C–H $\cdots \pi$ interactions in the packing structures have some changes with the rise of temperature (Tables S4–S8). Moreover, the O–H \cdots N hydrogen bonds are also observed at 99–298 K, with the H \cdots N centroid distances of 2.04–2.10 Å

(Fig. S17). All these show that temperature variation have a formative effect on bond lengths, angles and weak interactions.

2.3. DFT studies

Theoretical calculations for the cations $[\text{Cu}(\text{PPh}_3)_2(\text{PmH})]^+$ (1a'), $[\text{Cu}(\text{DPEphos})(\text{PmH})]^+$ (2a'), $[\text{Cu}(\text{Xantphos})(\text{PmH})]^+$ (3a'), and complexes $[\text{Cu}(\text{PPh}_3)_2(\text{Pm})]$ (1b), $[\text{Cu}(\text{DPEphos})(\text{Pm})]$ (2b), $[\text{Cu}(\text{Xantphos})(\text{Pm})]$ (3b) are used for the observation of electronic properties and Mülliken analysis (the luminescence of complexes 1a–3a are related to the cations 1a'–3a'). As presented in Tables 2 and S9, the HOMO \rightarrow LUMO energies of cations 1a'–3a' are in the range of 2.04–2.26 eV, which decreases the HOMO \rightarrow LUMO energy gap (0.36–0.57 eV) in contrast with that of neutral complexes 1b–3b. As previously reported [44], all these are partially because the deprotonation of PmH leads to the change of the charge distribution of copper(I) complexes. That is to say, the deprotonation of PmH may have great effects upon the HOMO \rightarrow LUMO energy gap, which provide valuable information on structure–property relation. Moreover, the HOMO \rightarrow LUMO energy gap of complex 1b shows almost no differences at 99–298 K (Table S9), implying that the HOMO–LUMO gap of this complex may be independent of the temperature.

As previously reported [45], DOS and PDOS can be used for observing the constituents of the HOMO and LUMO orbitals (DOS and PDOS below/above Fermi level would be related to HOMO/LUMO). In cation $[\text{Cu}(\text{PPh}_3)_2(\text{PmH})]^+$, the s orbitals from H, C, N and P atoms, the p orbitals from C, N and P atoms as well as the d orbitals from P and Cu atoms are the most contributions of the HOMOs, while the essential component of LUMOs are the p orbitals from C, N and P atoms, and a bit contribution of the p and d orbitals from P and Cu atom (Fig. S18). Meanwhile, the HOMO orbitals of $[\text{Cu}(\text{DPEphos})(\text{PmH})]^+$ and $[\text{Cu}(\text{Xantphos})(\text{PmH})]^+$ are mainly contributed by the s orbitals from H, C, N, O and P atoms, the p orbitals from C, N, O and P atoms, and the d orbitals of P and Cu atoms, while the largest contribution of LUMOs are the p orbitals from C, N, O and P atoms, and the p and d orbitals from P and Cu atoms (Figs. S19–S21). Because of luminescent properties of 1a–3a mainly having correlation with their cations, consequently, the HOMOs of 1a–3a are mostly delocalized over the copper d -orbital with phosphine character (1a: PPh₃; 2a: DPEphos; 3a: Xantphos), while the LUMOs are primarily located on PmH with admixed copper d -orbital to some extent (Table 3).

Different from 1a–3a, calculation results demonstrate that the largest contributions for the HOMOs of 1b–3b are the copper d -orbital and Pm

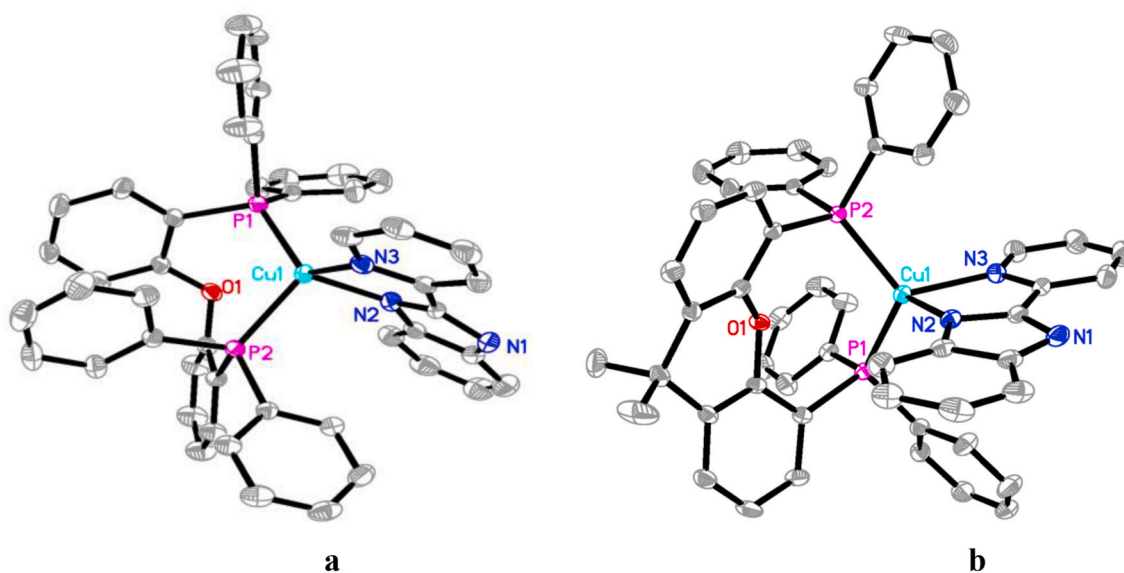


Fig. 4. Molecular structures of 2b (a) and 3b (b). The hydrogens are deleted for clarity.

Table 1

The selection of bond lengths (Å) and angles (°) for 1b under different temperatures.

	99 K	150 K	200 K	250 K	298 K
Cu1–P1	2.2457 (10)	2.2491 (13)	2.2486 (9)	2.2511 (9)	2.2532 (9)
Cu1–P2	2.2456 (10)	2.2510 (13)	2.2525 (9)	2.2565 (9)	2.2600 (9)
Cu1–N2	2.021 (3)	2.028 (4)	2.028 (3)	2.030 (2)	2.030 (3)
Cu1–N3	2.132 (3)	2.137 (4)	2.139 (3)	2.146 (3)	2.147 (3)
P2–Cu1–P1	118.74 (4)	119.04 (5)	119.22 (3)	119.43 (3)	119.63 (3)
N2–Cu1–P1	113.04 (9)	112.86 (11)	112.70 (8)	112.48 (8)	112.38 (8)
N2–Cu1–P2	119.23 (9)	119.16 (12)	119.17 (8)	119.17 (8)	119.04 (8)
N2–Cu1–N3	80.95 (11)	80.72 (15)	80.67 (11)	80.82 (10)	80.79 (11)
N3–Cu1–P1	111.90 (8)	112.08 (10)	112.21 (8)	112.20 (7)	112.32 (8)
N3–Cu1–P2	105.85 (8)	105.70 (11)	105.53 (8)	105.36 (8)	105.23 (8)

Table 2

The HOMO and LUMO energy, and Energy gaps of complexes 1a'–3a', 2b and 3b

complex	HOMO/eV	LUMO/eV	ΔE /eV
1a'	−7.75	−5.49	2.26
2a'	−7.42	−5.37	2.06
3a'	−7.47	−5.43	2.04
2b	−4.55	−2.03	2.52
3b	−4.58	−1.97	2.61

(Tables 3 and 4), having a certain consistency with the investigated DOS and PDOS (Figs. S22–S25). Meanwhile, compared with DOS and PDOS, the largest contributions for the LUMOs are Pm for 1b, DPEphos for 2b, Xantphos and Pm for 3b, implying that phosphine ligands have a

Table 3

Contour plots of the HOMO and LUMO of 1a'–3a', 2b and 3b

compound	HOMO	LUMO
1a'		
2a'		
3a'		
2b		
3b		

Table 4
Contour plots of the HOMO and LUMO of 1b at different temperatures.

Temperature	HOMO	LUMO
99 K		
150 K		
200 K		
250 K		
298 K		

Table 5
The selection of Mülliken atomic charges in 1a'-3a', 2b and 3b.

	1a'	2a'	3a'	2b	3b
	charges	charges	charges	charges	charges
Cu ₁	0.512	0.559	0.538	0.622	0.592
P ₁	0.771	0.780	0.798	0.769	0.791
P ₂	0.779	0.809	0.807	0.754	0.798
N ₂	-0.627	-0.616	-0.627	-0.696	-0.719
N ₃	-0.519	-0.535	-0.524	-0.534	-0.530

measurable effect on the component of the LUMOs. Moreover, as presented in Table 4 and Fig. S26, the ingredients of the HOMOs and LUMOs in 1b are virtually unchanged at 99–298 K, which is consistent with the minimal changes of bond lengths and angles under different temperatures (see Table 5).

As shown in Tables 5 and S10, Mülliken atomic charges of cations 1a'-3a' and compounds 1b-3b are calculated. For 1a'-3a', the charges of Cu atoms are in the range from 0.512 to 0.559, while corresponding

total charges of the coordinated atoms are -0.404 for 1a', -0.438 for 2a' and -0.454 for 3a'. All these suggest that phosphine ligands have a formative effect on atomic charges. Meanwhile, the charges of Cu atoms in 1b-3b are larger than the related values in cations 1a'-3a', respectively, which is probably caused by the deprotonation of PmH ligand. Furthermore, the charges of the copper atoms in 1a'-3a' and 1b-3b are less than +1, which may be beneficial for transfer charge of the copper atom and the enhancement of luminescent properties. In addition, Mülliken atomic charges of 1b at 99–298 K show that the charge of the copper atom is in the range from 0.562 to 0.569, and the variation in the total charges of the coordinated atoms at 99–298 K is going from 0.257 to 0.270 (Table S10). All these indicate that temperature variation may lead to the change of atomic charges, which may be also good for mediating charge migration and improving luminescent properties of the related copper(I) complexes.

2.4. Luminescent properties

As presented in Fig. 5 and Table 6, solid-state luminescent properties of cationic/neutral copper (I) complexes are observed at room temperature. For these copper (I) complexes with identical PmH/Pm ligands but different phosphine ligands, the tendency toward decreased quantum yield and phosphorescent lifetime, as well as for a red-shifted emission, goes with the size and steric encumbrance of phosphine ligands (The reason for this is that the size and steric encumbrance of phosphine ligands can tune structural relaxation in the CT excited state [23]). All these imply that the size and steric encumbrance of phosphine ligands have an important influence on luminescent properties of cationic/neutral copper (I) complexes. In addition, the emission peaks of cationic copper (I) complexes 1a, 2a and 3a are 534 nm, 569 nm and 566 nm, respectively, which may be tentatively assigned to metal-to-ligand charge transfer (MLCT) [19,46–48], consistent with the change of Mülliken atomic charges and the component of the HOMOs and LUMOs to some extent.

Meanwhile, the solid-state emissions of neutral copper (I) complexes 1b-3b have blue-shifted compared with cationic copper (I) complexes 1a-3a, implying that neutral structures have an important influence on luminescent properties of copper(I) complexes. Furthermore, The emission decay time of neutral copper (I) complexes (1b: $\tau = 137 \mu\text{s}$; 2b: $\tau = 17 \mu\text{s}$; 3b: $\tau = 8 \mu\text{s}$) are much larger than the corresponding values in cationic copper (I) complexes 1a-3a, which may partly be due to the deprotonation of PmH ligand leading to the change of charge migration. Simultaneously, quantum yield (Φ_{em}) in neutral copper (I) complexes 1b-3b reaches 42%, which is higher than [POPCu(FPhtpt)] [40] and [Cu(2PyN)(Xantphos)] [49], drastically increasing the quantum yield in comparison to that of the related cationic copper (I) complexes 1a-3a. Moreover, the K_{nr} values in these cationic/neutral copper (I) complexes are much more than the related Kr values (Table 6). All these show that the form of copper(I) complexes may have a strong effect on adapting and improving luminescent properties.

To observe the effect of temperature on solid-state luminescent properties, the photophysical properties of complex 1b are observed at 99–298 K. As shown in Fig. 6 and Table 7, the emission peaks of complex 1b range from 500 nm to 527 nm at 99 K to 520 nm at 298 K, while the excitation peaks vary from 420 nm to 460 nm at 99 K to 425 nm at 298 K. With the rise of temperature, the intensity of emission peaks will also decrease, coinciding with the change of the excitation peaks at different temperatures: (1) at 99–200 K, the emission peaks near 500 nm and 527 nm become much lower; (2) only the emission peak near 520 nm remain considerable strength at 250–298 K. Meanwhile, the emission decay time of complex 1b ranges from $\tau = 919 \mu\text{s}$ at 99 K to 297 μs at 298 K, suggesting that rising temperature can result in the decrease of phosphorescent lifetime. Furthermore, complex 1b has a rapid increase in the Kr and K_{nr} values with the increasement of temperature, and the variation of quantum yield, which ranges from $\Phi_{em} = 47\%$ at 99 K to 36% at 298 K, is unapparent. All these indicate that rising temperatures can

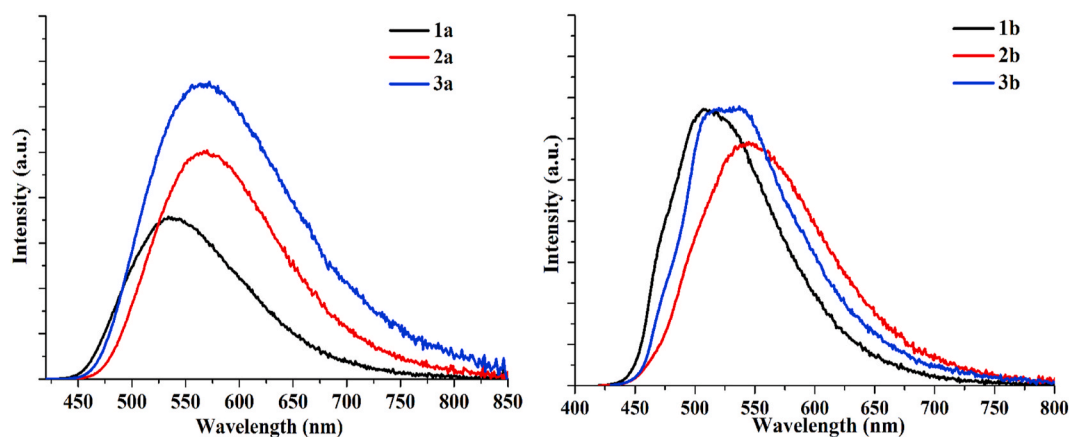


Fig. 5. Room-temperature, maximum emission spectra of 1a-3a (left) and 1b-3b (right).

Table 6

Room-temperature photophysical properties of six copper(I) compounds ($K_r = \Phi_{em}/\tau$; $K_{nr} = (1 - \Phi_{em})/\tau$ [13]).

	$\lambda_{max}(nm)$	$\tau(\mu s)$	$\Phi_{em}(\%)$	$K_r(s^{-1})$	$k_{nr}(s^{-1})$
1a	534 nm	10	26	2.60×10^4	7.40×10^4
2a	569 nm	7	27	3.86×10^4	1.04×10^5
3a	566 nm	0.5	1	2.00×10^4	1.98×10^5
1b	510 nm	137	42	3.07×10^3	4.23×10^3
2b	544 nm	17	25	1.47×10^4	4.41×10^4
3b	530 nm	8	17	2.13×10^4	1.04×10^5

result in the increasing of K_r and K_{nr} , and the decrease of phosphorescent lifetime and quantum yield.

2.5. Performance of LED devices

To observe potential application of copper (I) complexes, the monochromatic LED devices are manufactured by near-ultraviolet chips with cationic/neutral copper (I) complexes. As presented in Fig. 7, the EL spectra of the LED-a1, LED-a2 and LED-a3 devices show respectively the existence of the emission peaks near 537 nm, 560 nm and 570 nm, coinciding with the solid-state emission of cationic copper (I) complexes. Meanwhile, the LED-a1 device emit the yellow-green light with the CIE color coordinates of (0.3715, 0.5215), driven by 20 mA, while the LED-a2 and LED-a3 devices show the yellow light with the CIE coordinates of (0.4391, 0.5228) and (0.4458, 0.4973), respectively, under 20 mA driven current (Fig. 7 and Tables S11–S13). Notably, the EL intensity of the LED-a1, LED-a2 and LED-a3 devices are obviously

strengthened with the increment of current from 20 mA to 120 mA (Fig. 7). By comparing to the LED-a2 and LED-a3 devices, the LED-a1 device show better luminescence performance (Tables S11–S13): (1) the maximal external quantum efficiency (EQE) of the LED-a1 device is 7.10% and far greater than the corresponding values in the LED-a2 (6.14%) and LED-a3 device (1.98%); (2) the luminance efficiency (LE) is $LE_{(LED-a1)} > LE_{(LED-a2)} > LE_{(LED-a3)}$. Moreover, the CCT and CRI are 4809–4898 K and 50.7–50.8 for the LED-a1 device, 3717–3743 K and 50.2–50.7 for the LED-a2 device, as well as 3489–3571 K and 65.3–65.8 for the LED-a3 device (Tables S11–S13). All these indicate that complex 1 may be fit for acting as a yellow-green emitting material in the monochromatic LED.

We took neutral complexes 1b–3b instead of cationic complexes 1a–3a to fabricate the LED-b1, LED-b2 and LED-b3 devices. Similarly, the EL

Table 7

The photophysical properties of compound 1b under different temperatures ($K_r = \Phi_{em}/\tau$; $K_{nr} = (1 - \Phi_{em})/\tau$ [13]).

	99 K	150 K	200 K	250 K	298 K
$\lambda_{max}(nm)$	495 nm, 527 nm	498 nm, 527 nm	500 nm, 527 nm	520 nm	516 nm
$\tau(\mu s)$	919	837	655	460	297
$\Phi_{em}(\%)$	47	45	43	42	36
$K_r(s^{-1})$	5.11×10^2	5.38×10^2	6.56×10^2	9.13×10^2	1.21×10^3
$k_{nr}(s^{-1})$	5.77×10^2	6.57×10^2	8.70×10^2	1.26×10^3	2.15×10^3

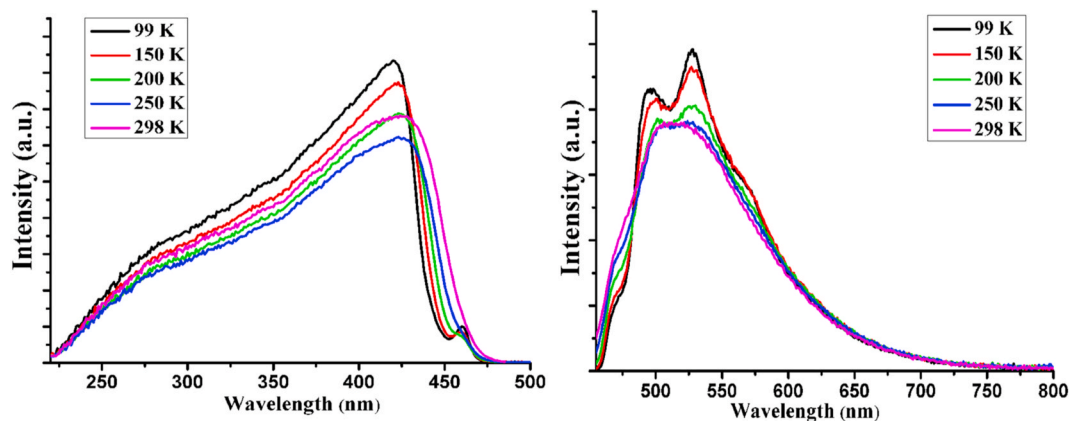


Fig. 6. (a) The maximum excitation spectra of 1b at the solid state, under different temperatures; (b) The maximum emission spectra of 1b at the solid state, under different temperatures.

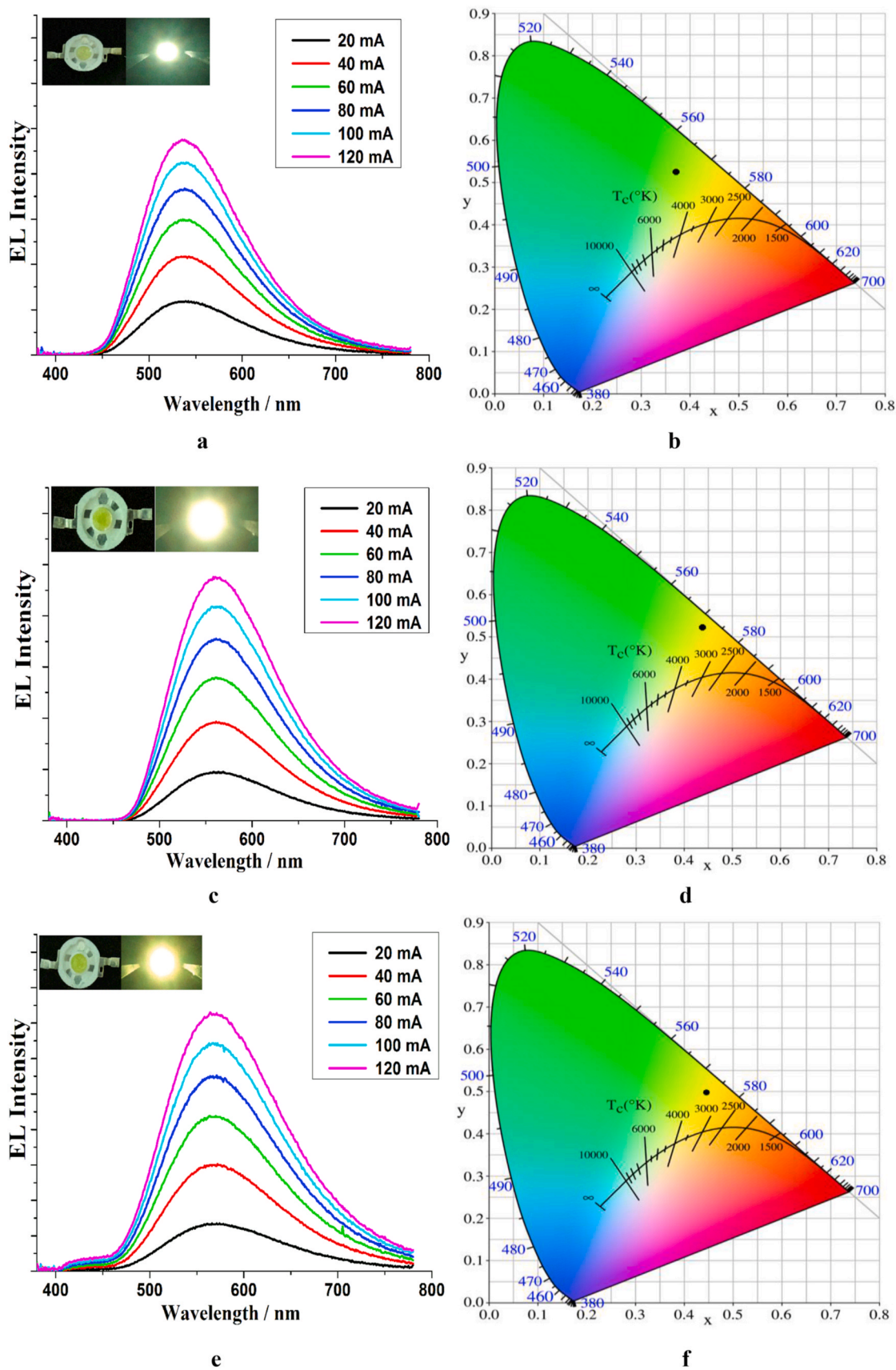


Fig. 7. (a) The EL spectra of LED-a1 made by 395 nm near-ultraviolet chip and complex 1a; (b) CIE chromaticity diagram of LED-a1, driven by 20 mA; (c) the EL spectra of LED-a2 made by 395 nm near-ultraviolet chip and complex 2a; (d) CIE chromaticity diagram of LED-a2, driven by 20 mA; (e) the EL spectra of LED-a3 made by 395 nm near-ultraviolet chip and complex 3a; (f) CIE chromaticity diagram of LED-a3, driven by 20 mA.

spectrums indicate two main emission peaks near 435 nm and 550 nm for the LED-b1 device, the emission peak of 555 nm for the LED-b2 device, and the emission peak near 565 nm for the LED-b3 device (Fig. 8). Under 20 mA driven current, the LED-b1 device show yellow-green emission with the CIE coordinates of (0.4029, 0.5072), while the LED-b2 and LED-b3 devices demonstrate respectively yellow emission with the CIE coordinates of (0.4074, 0.5125) and (0.4268, 0.5072) (Fig. 8). Meanwhile, the EL intensity of the LED-b1, LED-b2 and LED-b3 devices also increase with the rise of driven current from 20 mA to 120 mA. Compared with the previously observed LED-a1 and LED-a2 devices, the LED-b1 and LED-b2 devices show weaker luminescence: the maximal EQE (ca. 4.30%) and LE (ca. 12.33 lm/W) are much lower than the correlation values in the LED-a1 and LED-a2 devices (Tables S14–S15). Furthermore, the luminescence performance of the LED-b3 device is no obviously change compared to the LED-a3 device, and weaker than that of the LED-b1 and LED-b2 devices (Table S13–S16). These results show that the form of copper(I) complexes may be fundamental to their luminescence performance in the LED devices.

3. Conclusion

In summary, a series of cationic and neutral Cu(I) complexes have been prepared and characterized. On the basis of optimizing luminescent properties of Cu(I) complexes, the form of copper(I) complexes and the effect of temperature have been observed. For example, the studies of crystal structures, DFT calculation and photophysical properties of complex 1b at different temperatures show that temperature variation has a major impact on bond lengths and angles, weak interactions, Mülliken atom charges, phosphorescent lifetime and quantum yield. In these cationic and neutral Cu(I) complexes, the phosphorescent lifetime and quantum yield are up to 137 μ s and 42% at room temperature, respectively. Moreover, cationic and neutral Cu(I) complexes are used to fabricate the monochromatic LEDs, achieving favorable electroluminescence with the maximum EQE of 7.10%.

4. Experimental section

4.1. General procedures

All chemicals (A. R. grade) were purchased from Energy Chemical or Aladdin, and used without further purification. The PerkinElmer Frontier Near/Mid-IR Std spectrometer of 4000–400 cm^{-1} are used to observe IR spectra. ^1H , ^{13}C and $^{31}\text{P}\{^1\text{H}\}$ spectra were determined by using a Bruker AVANCE-500/600 spectrometer. The crystal phases and elemental analyses are measured by the Bruker D2 PHASER X-ray diffractometer and Vario EL Cube elemental analyzer, respectively. The luminescent spectra as well as emission lifetime were collected using an Edinburgh Instruments FLS980 spectrophotometer. Room-temperature emission quantum yields were recorded on a HORIBA Dual-FL spectrophotometer with PL quantum yield measurement system.

The luminescent spectra and emission lifetime of compound 1b at different temperatures are observed using a temperature controller (LNP95, Linkam) attached to FLS980 spectrophotometer, while emission quantum yields are measured by a self-developed absolute PL quantum yield measurement system (a self-developed integrating sphere, a LNP95 temperature controller and a QEPs spectrometer). Performance of the LED devices are collected on a Everfine Instruments HAAS2000 LED optoelectronic analyzer.

4.1.1. Synthetic method

The mixture of $[\text{Cu}(\text{CH}_3\text{CN})_4]\text{BF}_4$ and phosphine ligand (1a: PPh_3 ; 2a: DPEphos ; 3a: Xantphos) in 5 mL of acetonitrile was stirred for 20 min and then PmH was added. After reaction, the acetonitrile solvent was evaporated to give cationic compounds 1a–3a. Meanwhile, reacting cationic compounds 1a–3a with KOH (2 equiv.) in 5 mL of acetonitrile/methanol produced the precipitation of neutral Cu(I) complexes 1b–3b,

and then the relative complexes were obtained by filtration. Furthermore, the crystals of compounds 1a, 2a, 3a, 2b and 3b were obtained by the diffusion of n-hexane into the CH_2Cl_2 or CHCl_3 solution of the related Cu(I) complexes, except that the crystal of compound 1b was offered by recrystallization from ethanol.

4.1.2. $[\text{Cu}(\text{PPh}_3)_2(\text{PmH})]\text{BF}_4$ (1a)

Yield: 0.0398 g (ca.46%). IR (cm^{-1}): 3235 (br), 3052 (m), 1601(w), 1478 (m), 1435 (s), 1319 (w), 1094(s), 994 (vs), 796 (w), 742 (s), 694 (s), 516(s). ^1H NMR (600.13 MHz, CDCl_3 , 25 $^\circ\text{C}$, TMS): δ = 7.02–7.07 (m, 12H), 7.09 (t, J = 7.6 Hz, 13H), 7.12–7.18 (m, 2H), 7.19 (s, 1H), 7.23–7.28 (m, 7H), 7.82 (d, J = 8.2 Hz, 1H), 7.87 (t, J = 7.8 Hz, 1H), 8.06 (d, J = 5.1 Hz, 1H), 8.40 (d, J = 8.1 Hz, 1H). ^{13}C NMR (125.75 MHz, CDCl_3) δ = 149.4, 148.7, 145.5, 140.4, 138.9, 135.4, 133.1, 132.5, 132.4, 130.1, 128.8, 125.5, 125.2, 123.7, 123.0, 117.9, 114.4. $^{31}\text{P}\{^1\text{H}\}$ -NMR (242.94 MHz, CDCl_3 , 25 $^\circ\text{C}$, TMS): 1.86 ppm. Elemental analysis: calculated for $\text{C}_{48}\text{H}_{39}\text{BCuF}_4\text{N}_3\text{P}_2$: C 66.26, H 4.52, N 4.83. Found C 65.96, H 4.77, N 4.64.

4.1.3. $[\text{Cu}(\text{DPEphos})(\text{PmH})]\text{BF}_4$ (2a)

Yield: 0.0516 g (ca.58%). IR (cm^{-1}): 3434 (br), 3243(m), 3054 (m), 1588(w), 1479 (w), 1436 (vs), 1319 (w), 1260(m), 1217(s), 1095(s), 988 (m), 793 (w), 743 (s), 695 (s), 502(s). ^1H NMR (600.13 MHz, CDCl_3 , 25 $^\circ\text{C}$, TMS): δ = 6.86–7.00 (m, 10H), 7.07 (t, J = 7.7 Hz, 1H), 7.10–7.15 (m, 10H), 7.22–7.28 (m, 10H), 7.29–7.35 (m, 1H), 7.43–7.51 (m, 1H), 7.83 (d, J = 8.2 Hz, 1H), 7.90 (t, J = 7.7 Hz, 1H), 8.14 (d, J = 5.2 Hz, 1H), 8.47 (d, J = 8.1 Hz, 1H). ^{13}C NMR (125.75 MHz, CDCl_3) δ = 158.6, 149.2, 148.6, 145.4, 140.5, 138.7, 135.3, 134.3, 133.4, 132.7, 131.6, 130.1, 129.9, 128.6, 125.2, 125.0, 124.9, 124.7, 123.5, 122.8, 120.2, 117.7, 114.2. $^{31}\text{P}\{^1\text{H}\}$ -NMR (242.94 MHz, CDCl_3 , 25 $^\circ\text{C}$, TMS): –11.86 ppm. Elemental analysis: calculated for $\text{C}_{48}\text{H}_{37}\text{BCuF}_4\text{N}_3\text{OP}_2$: C 65.21, H 4.22, N 4.75. Found C 64.89, H 4.59, N 4.41.

4.1.4. $[\text{Cu}(\text{Xantphos})(\text{PmH})]\text{BF}_4$ (3a)

Yield: 0.0621 g (ca.67%). IR (cm^{-1}): 3433 (br), 3264(m), 3051 (w), 2961(w), 1599(w), 1478 (m), 1437 (s), 1408 (vs), 1318 (w), 1243(m), 1082(s), 967 (w), 793 (m), 745 (vs), 695 (s), 508(s). ^1H NMR (600.13 MHz, CDCl_3 , 25 $^\circ\text{C}$, TMS): δ = 1.71 (s, 3H), 1.86 (s, 3H), 6.41 (d, J = 8.1 Hz, 1H), 6.53–6.57 (m, 2H), 6.84–6.87 (m, 4H), 7.03–7.16 (m, 13H), 7.19–7.30 (m, 9H), 7.64 (d, J = 8.1 Hz, 2H), 7.85 (d, J = 8.2 Hz, 1H), 7.94 (t, J = 7.9 Hz, 1H), 8.17 (d, J = 5.0 Hz, 1H), 8.53 (d, J = 8.1 Hz, 1H). ^{13}C NMR (125.75 MHz, CDCl_3) δ = 155.1, 155.0, 149.0, 148.7, 145.3, 140.5, 138.8, 135.3, 133.8, 132.9, 132.8, 132.7, 132.6, 131.9, 131.8, 131.7, 131.6, 131.2, 129.9, 129.8128.7, 126.9, 125.6, 125.0, 123.4, 123.0, 120.8, 120.7, 117.2, 114.2, 36.1, 29.7, 27.1. $^{31}\text{P}\{^1\text{H}\}$ -NMR (242.94 MHz, CDCl_3 , 25 $^\circ\text{C}$, TMS): –12.64 ppm. Elemental analysis: calculated for $\text{C}_{51}\text{H}_{41}\text{BCuF}_4\text{N}_3\text{OP}_2$: C 66.28, H 4.47, N 4.55. Found C 65.86, H 4.79, N 4.73.

4.1.5. $[\text{Cu}(\text{PPh}_3)_2(\text{Pm})]$ (1b)

Yield: 0.0139 g (ca.35%). IR (cm^{-1}): 3434 (br), 3050 (m), 1598(m), 1478 (m), 1434 (s), 1379 (m), 1328(m), 1279(m), 1093(s), 739 (vs), 693 (vs), 508(s). ^1H NMR (600.13 MHz, CDCl_3 , 25 $^\circ\text{C}$, TMS): δ = 7.04–7.36 (m, 33H), 7.46 (t, J = 8.0 Hz, 2H), 7.55 (t, J = 7.5 Hz, 1H), 7.65–7.69 (m, 2H). ^{13}C NMR (125.75 MHz, CD_3SOCD_3) δ = 158.6, 153.2, 149.2, 138.2, 134.1133.9, 133.4, 133.3, 132.5, 132.0, 131.9, 130.2, 130.0, 129.3, 129.2, 129.1, 129.0, 123.5, 121.5, 120.0, 118.6, 116.3. $^{31}\text{P}\{^1\text{H}\}$ -NMR (202.44 MHz, CD_3SOCD_3 , 25 $^\circ\text{C}$, TMS): –1.24 ppm. Elemental analysis: calculated for $\text{C}_{48}\text{H}_{38}\text{CuN}_3\text{P}_2$: C 73.69, H 4.90, N 5.37. Found C 73.42, H 5.26, N 5.05.

4.1.6. $[\text{Cu}(\text{DPEphos})(\text{Pm})]$ (2b)

Yield: 0.0273 g (ca.53%). IR (cm^{-1}): 3051 (m), 1600(m), 1563 (w), 1462 (m), 1434 (vs), 1383 (s), 1329 (m), 1275(m), 1220(s), 1145 (s), 1095(s), 1068 (w), 793 (w), 744 (s), 695 (s), 507(s). ^1H NMR (600.13 MHz, CDCl_3 , 25 $^\circ\text{C}$, TMS): δ = 6.77 (s, 2H), 6.85 (s, 1H), 6.91 (s, 3H),

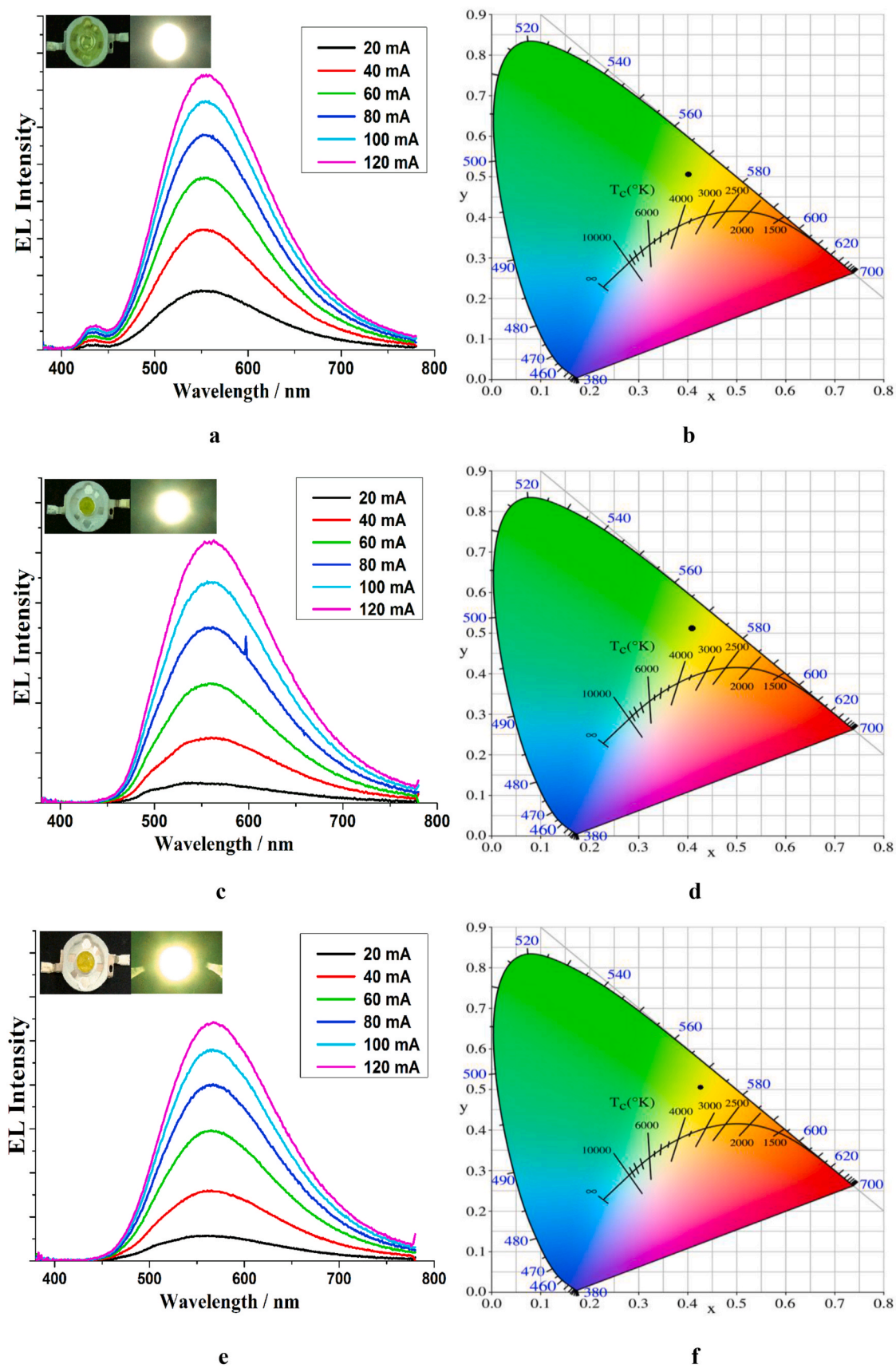


Fig. 8. (a) The EL spectra of LED-b1 made by 395 nm near-ultraviolet chip and compound 1b; (b) CIE chromaticity diagram of LED-b1, driven by 20 mA; (c) the EL spectra of LED-b2 made by 395 nm near-ultraviolet chip and compound 2b; (d) CIE chromaticity diagram of LED-b2, driven by 20 mA; the EL spectra of LED-b3 made by 395 nm near-ultraviolet chip and compound 3b; (f) CIE chromaticity diagram of LED-b3, driven by 20 mA.

6.99–7.27 (m, 25H), 7.33 (d, $J = 7.9$ Hz, 1H), 7.61–7.79 (m, 2H), 7.96 (s, 1H), 8.50 (s, 1H). ^{13}C NMR (125.75 MHz, CDCl_3) $\delta = 158.6, 158.5, 158.2, 153.0, 148.3, 147.8, 145.2, 136.8, 134.3, 133.5, 132.5, 131.1, 129.4, 129.3, 128.3, 128.2, 125.8, 125.7, 125.6, 124.5, 122.1, 121.3, 120.3, 119.7, 119.5, 118.0, 116.6$. $^{31}\text{P}\{^1\text{H}\}$ -NMR (242.94 MHz, CDCl_3 , 25 °C, TMS): -13.73 ppm. Elemental analysis: calculated for $\text{C}_{48}\text{H}_{36}\text{CuN}_3\text{OP}_2$: C 72.40, H 4.56, N 5.28. Found C 72.63, H 4.96, N 4.82.

4.1.7. [Cu(Xantphos) (Pm)] (3b)

Yield: 0.0285 g (ca.46%). 3434 (br), 3042 (w), 2951 (w), 1596(m), 1479 (m), 1435 (m), 1408 (s), 1375(w), 1325(m), 1237(m), 1025(w), 975 (w), 793 (w), 742 (vs), 694 (s), 511(s). ^1H NMR (600.13 MHz, CDCl_3 , 25 °C, TMS): $\delta = 1.70$ (s, 3H), 1.87 (s, 3H), 6.35 (d, $J = 7.7$ Hz, 1H), 6.39–6.43 (m, 2H), 6.64 (t, $J = 7.6$ Hz, 1H), 6.95 (s, 5H), 6.97–7.16 (m, 16H), 7.19 (t, $J = 7.5$ Hz, 2H), 7.26 (s, 1H), 7.58 (d, $J = 7.8$ Hz, 2H), 7.69 (t, $J = 7.7$ Hz, 1H), 7.75 (d, $J = 8.0$ Hz, 1H), 8.02 (d, $J = 4.8$ Hz, 1H), 8.57 (s, 1H). ^{13}C NMR (125.75 MHz, CDCl_3) $\delta = 158.4, 155.4, 155.3, 153.4, 148.2, 145.3, 136.8, 133.7, 133.5, 133.4, 133.3, 133.2, 133.1, 133.0, 131.1, 129.2, 129.1, 128.3, 126.1, 124.0, 122.2, 122.0, 121.9, 121.8, 121.5, 119.4, 119.3, 118.3, 115.9, 36.1, 29.7, 26.8$. $^{31}\text{P}\{^1\text{H}\}$ -NMR (242.94 MHz, CDCl_3 , 25 °C, TMS): -13.67 ppm. Elemental analysis: calculated for $\text{C}_{51}\text{H}_{40}\text{CuN}_3\text{OP}_2$: C 73.24, H 4.82, N 5.02. Found C 73.02, H 5.16, N 4.87.

4.2. X-ray crystallography

The single crystal X-ray diffraction data of cationic and neutral Cu(I) complexes (1a–3a and 1b–3b) were recorded using graphite monochromated Mo-K α radiation ($\lambda = 0.71073$ Å) on a Bruker D8 Adventure diffractometer. Meanwhile, the crystallographic data of compound 1b were collected at 99–298 K. The related crystal structures were solved by direct or patterson methods, and refined with the full-matrix least-squares on F^2 using SHELXTL and the olex2refine refinement package. No hydrogen atoms are arranged on O2 in 2a and 2b. In the structure refinement of compound 3a, the unidentifiable and badly disordered solvent molecules (probably H_2O) are omitted by the squeeze option in PLATON. Crystallographic data for these six compounds are shown in Tables S1–S2. The selection of bond lengths and bond angles are presented in Tables 1 and S3.

4.3. Computational section

The mGGA-DFT functional of the DMol 3 module is used to perform DFT calculations of $[\text{Cu}(\text{PPh}_3)_2(\text{PmH})]^+(1a')$, $[\text{Cu}(\text{DPEphos})(\text{PmH})]^+(2a')$, $[\text{Cu}(\text{Xantphos})(\text{PmH})]^+(3a')$, $[\text{Cu}(\text{PPh}_3)_2(\text{Pm})]$ (1b), $[\text{Cu}(\text{DPEphos})(\text{Pm})]$ (2b) and $[\text{Cu}(\text{Xantphos})(\text{Pm})]$ (3b). Meanwhile, the local function for the exchange correlation potential and basis set are meta-GGA M11-L and DND, respectively. Moreover, in the calculation process, the relevant parameters are set (SCF tolerance: 10^{-5} ; max. force: 0.004 Ha Å^{-1} ; max. displacement: 0.005 Å; convergence tolerances for energy tolerances change: 2.0×10^{-5} Ha).

4.4. Fabrication of the LEDs devices

The monochromatic LED devices are manufactured by using a near-ultraviolet chip ($\lambda_{\text{em}} = 395$ nm) as the excitation source, while complexes 1a, 2a, 3a, 1b, 2b and 3b were used as the yellow/yellow-green phosphors. The proper amounts of complexes 1a, 2a, 3a, 1b, 2b and 3b were completely mixed with epoxy resins, respectively, and the related mixtures were coated on the near-ultraviolet chips to obtain the monochromatic LED devices [50–52]. The monochromatic LED devices were driven by various currents (20–120 mA). The EL spectra, correlated color temperature (CCT), colour rendering index (CRI), luminance efficiency (LE) and external quantum efficiency (EQE) were measured on a Everfine Instruments HAAS2000 LED optoelectronic analyzer.

Declaration of competing interest

We declare that we have no financial and personal relationships with other people or organizations that could inappropriately influence (bias) their work or state.

Acknowledgements

DFT calculations are supported by High performance computing center of science & engineering of Sichuan University of Science & Engineering.

Appendix A. Supplementary data

Supplementary data to this article can be found online at <https://doi.org/10.1016/j.orgel.2021.106273>.

References

- [1] M. Bachmann, O. Blacque, K. Venkatesan, Harnessing white-light luminescence via tunable singlet- and triplet-derived emissions based on gold(III) complexes, *Chem. Eur. J.* 23 (2017) 9451–9456.
- [2] M.V. Bobo, A. Paul, A.J. Robb, A.M. Arcidiacono, M.D. Smith, K. Hanson, A. K. Vannucci, Bis-cyclometalated iridium complexes containing 4, 4'-bis (phosphonomethyl)-2, 2'-bipyridine ligands: photophysics, electrochemistry, and high-voltage dye-sensitized solar cells, *Inorg. Chem.* 59 (2020) 6351–6358.
- [3] F. Chotard, V. Sivchik, M. Linnolahti, M. Bochmann, A.S. Romanov, Mono- versus bicyclic carbene metal amide photoemitters: which design leads to the best performance? *Chem. Mater.* 32 (2020) 6114–6122.
- [4] X. Feng, Y. Feng, N. Guo, Y. Sun, T. Zhang, L. Ma, L. Wang, Series d-f heteronuclear metal-organic frameworks: color tunability and luminescent probe with switchable properties, *Inorg. Chem.* 56 (2017) 1713–1721.
- [5] G. Li, D. Zhu, X. Wang, Z. Su, M.R. Bryce, Dinuclear metal complexes: multifunctional properties and applications, *Chem. Soc. Rev.* 49 (2020) 765–838.
- [6] B.-F. Long, M.-F. Wang, Q. Huang, X.-H. Yin, D.J. Young, F.-L. Hu, Y. Mi, A pillar-layer strategy to construct 2D polycatenated coordination polymers for luminescence detection of $\text{Cr}_2\text{O}_7^{2-}$ and CrO_4^{2-} in aqueous solution, *CrystEngComm* 21 (2019) 4943–4950.
- [7] T. Oshima, S. Nishioka, Y. Kikuchi, S. Hirai, K.-i. Yanagisawa, M. Eguchi, Y. Miseki, T. Yokoi, T. Yui, K. Kimoto, K. Sayama, O. Ishitani, T.E. Mallouk, K. Maeda, An artificial Z-scheme constructed from dye-sensitized metal oxide nanosheets for visible light-driven overall water splitting, *J. Am. Chem. Soc.* 142 (2020) 8412–8420.
- [8] H.K. Saeed, S. Sreedharan, P.J. Jarman, S.A. Archer, S.D. Fairbanks, S.P. Foxon, A. J. Auty, D. Chekulaev, T. Keane, A.J.H.M. Meijer, J.A. Weinstein, C.G.W. Smythe, J. Bernardino de la Serna, J.A. Thomas, Making the Right Link to Theranostics: the photophysical and biological properties of dinuclear $\text{Ru}^{\text{II}}\text{-Re}^{\text{I}}$ dppz complexes depend on their tether, *J. Am. Chem. Soc.* 142 (2020) 1101–1111.
- [9] M. Elie, F. Sguerra, F. Di Meo, M.D. Weber, R. Marion, A. Grimault, J.-F. Lohier, A. Stallivieri, A. Brosseau, R.B. Pansu, J.-L. Renaud, M. Linares, M. Hamel, R. D. Costa, S. Gaillard, Designing NHC-copper(I) dipyrrolylamine complexes for blue light-emitting electrochemical cells, *ACS Appl. Mater. Interfaces* 8 (2016) 14678–14691.
- [10] K. Lee, P.-N. Lai, R. Parveen, C.M. Donahue, M.M. Wymore, B.A. Massman, B. Vlasisavljevic, T.S. Teets, S.R. Daly, Modifying the luminescent properties of a Cu(I) diphosphine complex using ligand-centered reactions in single crystals, *Chem. Commun.* 56 (2020) 9110–9113.
- [11] J.-X. Li, Z.-X. Du, L.-L. Zhang, D.-L. Liu, Q.-Y. Pan, Doubly mononuclear cocrystal and oxalato-bridged binuclear copper compounds containing flexible 2-(3,5,6-trichloropyridin-2-yl) oxy)acetate tectons: synthesis, crystal analysis and magnetic properties, *Inorg. Chim. Acta.* 512 (2020), 119890.
- [12] A. Schinabeck, M.J. Leitl, H. Yersin, Dinuclear Cu(I) Complex with combined bright TADF and phosphorescence. Zero-Field splitting and spin-lattice relaxation effects of the triplet state, *J. Phys. Chem. Lett.* 9 (2018) 2848–2856.
- [13] R. Czerwieńec, K. Kowalski, H. Yersin, Highly efficient thermally activated fluorescence of a new rigid Cu(I) complex $[\text{Cu}(\text{dmp})(\text{phanephos})]^+$, *Dalton Trans.* 42 (2013) 9826–9830.
- [14] F. Wu, J. Li, H. Tong, Z. Li, C. Adachi, A. Langlois, P.D. Harvey, L. Liu, W.-Y. Wong, W.-K. Wong, X. Zhu, Phosphorescent Cu(I) complexes based on bis(pyrazol-1-yl-methyl)-pyridine derivatives for organic light-emitting diodes, *J. Mater. Chem. C* 3 (2015) 138–146.
- [15] M. Hashimoto, S. Igawa, M. Yashima, I. Kawata, M. Hoshino, M. Osawa, Highly efficient green organic light-emitting diodes containing luminescent three-coordinate copper(I) complexes, *J. Am. Chem. Soc.* 133 (2011) 10348–10351.
- [16] M.D. Weber, E. Fresta, M. Elie, M.E. Miehlich, J.-L. Renaud, K. Meyer, S. Gaillard, R.D. Costa, Rationalizing fabrication and design toward highly efficient and stable blue light-emitting electrochemical cells based on NHC copper(I) complexes, *Adv. Funct. Mater.* 28 (2018), 1707423.

- [17] D.M. Zink, D. Volz, T. Baumann, M. Mydlak, H. Flüggé, J. Friedrichs, M. Nieger, S. Bräse, Heteroleptic, dinuclear copper(I) complexes for application in organic light-emitting diodes, *Chem. Mater.* 25 (2013) 4471–4486.
- [18] R. Hamze, J.L. Peltier, D. Sylvinson, M. Jung, J. Cardenas, R. Haiges, M. Soleilhavoup, R. Jazzar, P.I. Djurovich, G. Bertrand, M.E. Thompson, Eliminating nonradiative decay in Cu(I) emitters: >99% quantum efficiency and microsecond lifetime, *Science* 363 (2019) 601–606.
- [19] J. Min, Q. Zhang, W. Sun, Y. Cheng, L. Wang, Neutral copper(I) phosphorescent complexes from their ionic counterparts with 2-(2'-quinolyl)benzimidazole and phosphine mixed ligands, *Dalton Trans.* 40 (2011) 686–693.
- [20] T.J. Penfold, S. Karlsson, G. Capano, F.A. Lima, J. Rittmann, M. Reinhard, M. H. Rittmann-Frank, O. Braem, E. Baranoff, R. Abela, I. Tavernelli, U. Rothlisberger, C.J. Milne, M. Chergui, Solvent-induced luminescence quenching: static and time-resolved X-Ray absorption spectroscopy of a copper(I) phenanthroline complex, *J. Phys. Chem.* 117 (2013) 4591–4601.
- [21] L. Ravotto, P. Ceroni, Aggregation induced phosphorescence of metal complexes: from principles to applications, *Coord. Chem. Rev.* 346 (2017) 62–76.
- [22] R. Utrera-Melero, J.-Y. Mevellec, N. Gautier, N. Stephant, F. Massuyeau, S. Perruchas, Aggregation-induced emission properties of copper iodide clusters, *Chem. Asian J.* 14 (2019) 3166–3172.
- [23] R. Hou, T.-H. Huang, X.-J. Wang, X.-F. Jiang, Q.-L. Ni, L.-C. Gui, Y.-J. Fan, Y.-L. Tan, Synthesis, structural characterization and luminescent properties of a series of Cu(I) complexes based on polyphosphine ligands, *Dalton Trans.* 40 (2011) 7551–7558.
- [24] Y. Shi, X. Liu, Y. Shan, X. Zhang, W. Kong, Y. Lu, Z. Tan, X.-L. Li, Naked-eye repeatable off-on-off and on-off-on switching luminescence of copper(I)-1H-imidazo[4,5-f][1,10]phenanthroline complexes with reversible acid-base responses, *Dalton Trans.* 48 (2019) 2430–2441.
- [25] X.-L. Xin, M. Chen, Y.-b. Ai, F.-I. Yang, X.-L. Li, F. Li, Aggregation-Induced emissive copper(I) complexes for living cell imaging, *Inorg. Chem.* 53 (2014) 2922–2931.
- [26] M. Gernert, L. Balles-Wolf, F. Kerner, U. Müller, A. Schmiedel, M. Holzapfel, C. M. Marian, J. Pflaum, C. Lambert, A. Steffen, Cyclic (Amino)(aryl)carbenes enter the field of chromophore ligands: expanded π system leads to unusually deep red emitting CuI compounds, *J. Am. Chem. Soc.* 142 (2020) 8897–8909.
- [27] A.V. Artem'ev, M.P. Davydova, A.S. Berezin, M.R. Ryzhikov, D.G. Samsonenko, Dicopper(I) paddle-wheel complexes with thermally activated delayed fluorescence adjusted by ancillary ligands, *Inorg. Chem.* 59 (2020) 10699–10706.
- [28] A.Y. Baranov, A.S. Berezin, D.G. Samsonenko, A.S. Mazur, P.M. Tolstoy, V. F. Plyusnin, I.E. Kolesnikov, A.V. Artem'ev, New Cu(I) halide complexes showing TADF combined with room temperature phosphorescence: the balance tuned by halogens, *Dalton Trans.* 49 (2020) 3155–3163.
- [29] H. Kitagawa, Y. Ozawa, K. Toriumi, Flexibility of cubane-like Cu₄L₄ framework: temperature dependence of molecular structure and luminescence thermochromism of [Cu₄L₄(PPh₃)₄] in two polymorphic crystalline states, *Chem. Commun.* 46 (2010) 6302–6304.
- [30] M. Olaru, E. Rychagova, S. Ketkov, Y. Shynkarenko, S. Yakunin, M.V. Kovalenko, A. Yablonskiy, B. Andreev, F. Kleemiss, J. Beckmann, M. Vogt, A Small cationic organo-copper cluster as thermally robust highly photo- and electroluminescent material, *J. Am. Chem. Soc.* 142 (2020) 373–381.
- [31] C.M. Brown, V. Carta, M.O. Wolf, Thermochromic solid-state emission of dipyrrolyl sulfoxide Cu(I) complexes, *Chem. Mater.* 30 (2018) 5786–5795.
- [32] S. Evariste, A.M. Khalil, M.E. Moussa, A.K.-W. Chan, E.Y.-H. Hong, H.-L. Wong, B. Le Guennic, G. Calvez, K. Costuas, V.W.-W. Yam, C. Lescop, Adaptive coordination-driven supramolecular syntheses toward new polynuclear Cu(I) luminescent assemblies, *J. Am. Chem. Soc.* 140 (2018) 12521–12526.
- [33] T.-H. Huang, Q.-L. Hu, F.-Z. Zhao, D. Zheng, Q. Liu, T.-C. Wu, C. Luo, L.-C. Gui, J. Chen, Structural characterization, electronic and luminescent properties of copper(I) complexes with different temperatures and their application to light-emitting diodes, *J. Lumin.* 227 (2020), 117530.
- [34] T. Hou, J. Bian, X. Yue, S. Yue, J. Ma, Synthesis, crystal structure, photoluminescence and theoretical studies of a series of copper(I) compounds based on imidazole derivatives, *Inorg. Chim. Acta.* 394 (2013) 15–20.
- [35] R. Horvath, M.G. Fraser, S.A. Cameron, A.G. Blackman, P. Wagner, D.L. Officer, K. C. Gordon, Synthesis, characterization, and photophysics of oxadiazole- and diphenylamine-substituted Re(I) and Cu(I) complexes, *Inorg. Chem.* 52 (2013) 1304–1317.
- [36] C.M. Brown, C. Li, V. Carta, W. Li, Z. Xu, P.H.F. Stroppa, I.D.W. Samuel, E. Zysman-Colman, M.O. Wolf, Influence of sulfur oxidation state and substituents on sulfur-bridged luminescent copper(I) complexes showing thermally activated delayed fluorescence, *Inorg. Chem.* 58 (2019) 7156–7168.
- [37] M. Washimi, M. Nishikawa, N. Shimoda, S. Satokawa, T. Tsubomura, Blue and orange oxygen responsive emissions in the solid state based on copper(I) complexes bearing dodecafluorinated diphosphine and 1,10-phenanthroline derivative ligands, *Inorg. Chem. Frontiers* 4 (2017) 639–649.
- [38] T.-H. Huang, M.-H. Zhang, C.-Y. Gao, L.-T. Wang, Synthesis, structures and characterization of metal complexes containing 4'-phenyl-2,2':6',2''-terpyridine ligands with extended π - π interactions, *Inorg. Chim. Acta.* 408 (2013) 91–95.
- [39] M. Nishio, M. Hirota, Y. Umezawa, The CH/ π Interaction: Evidence, Nature, and Consequences, Wiley-VCH, Weinheim, 1998.
- [40] Y. Sun, V. Lemaire, J.I. Beltrán, J. Cornil, J. Huang, J. Zhu, Y. Wang, R. Fröhlich, H. Wang, L. Jiang, G. Zou, Neutral mononuclear copper(I) complexes: synthesis, crystal structures, and photophysical properties, *Inorg. Chem.* 55 (2016) 5845–5852.
- [41] K.J. Lotito, J.C. Peters, Efficient luminescence from easily prepared three-coordinate copper(I) arylamidophosphines, *Chem. Commun.* 46 (2010) 3690–3692.
- [42] T.-H. Huang, M.-H. Zhang, J. Yan, H. Yang, S.-X. Hao, C.-L. Zhang, Synthesis, structure, characterization and luminescent properties of copper(I) complexes based on bis-diimine bridging ligands, *Inorg. Chim. Acta.* 437 (2015) 47–53.
- [43] E. Leoni, J. Mohanraj, M. Holler, M. Mohankumar, I. Nierengarten, F. Monti, A. Sournia-Saquet, B. Delavaux-Nicot, J.-F. Nierengarten, N. Armaroli, Heteroleptic copper(I) complexes prepared from phenanthroline and bis-phosphine ligands: rationalization of the photophysical and electrochemical properties, *Inorg. Chem.* 57 (2018) 15537–15549.
- [44] X. Liu, R. Li, L. Ma, X. Feng, Y. Ding, Influences of the protonic state of an imidazole-phenanthroline ligand on the luminescence properties of copper(I) complexes: experimental and theoretical research, *New J. Chem.* 40 (2016) 619–625.
- [45] T.-H. Huang, J.-Q. Liu, H. Yang, B. Zhao, J. Shang, Synthesis, structural characterization, DFT studies, and spectroscopic properties of copper(I) complexes with extended C-H \cdots π interactions, *Aust. J. Chem.* 69 (2016) 826–835.
- [46] L. Bergmann, J. Friedrichs, M. Mydlak, T. Baumann, M. Nieger, S. Bräse, Outstanding luminescence from neutral copper(I) complexes with pyridyl-tetrazolate and phosphine ligands, *Chem. Commun.* 49 (2013) 6501–6503.
- [47] A.C. Brannan, Y. Lee, Photophysical tuning of σ -SiH copper-carbazole complexes to give deep-blue emission, *Inorg. Chem.* 59 (2020) 315–324.
- [48] A. Wada, Q. Zhang, T. Yasuda, I. Takasu, S. Enomoto, C. Adachi, Efficient luminescence from a copper(I) complex doped in organic light-emitting diodes by suppressing C-H vibrational quenching, *Chem. Commun.* 48 (2012) 5340–5342.
- [49] M.G. Crestani, G.F. Manbeck, W.W. Brennessel, T.M. McCormick, R. Eisenberg, Synthesis and characterization of neutral luminescent diphosphine pyrrole- and indole-aldimine copper(I) complexes, *Inorg. Chem.* 50 (2011) 7172–7188.
- [50] J. Huang, B. Su, E. Song, M.S. Molocheev, Z. Xia, Ultra-broad-band-excitable Cu(I)-based organometallic halide with near-unity emission for light-emitting diode applications, *Chem. Mater.* (2021), <https://doi.org/10.1021/acs.chemmater.1c00085>.
- [51] N. Ma, W. Li, B. Devakumar, Z. Zhang, X. Huang, Utilizing energy transfer strategy to produce efficient green luminescence in Ca₂LuHf₂Al₃O₁₂:Ce³⁺, Tb³⁺ garnet phosphors for high-quality near-UV-pumped warm-white LEDs, *J. Colloid Interface Sci.* 601 (2021) 365–377.
- [52] Y. Zhu, L. Fu, D. Wu, J. Peng, F. Du, X. Ye, L. Chen, W. Zhuang, A cyan-emitting phosphor Ca₃SiO₄(Cl,Br)₂:Eu²⁺ with high efficiency and good thermal stability for full-visible-spectrum LED lighting, *J. Lumin.* 232 (2021), 117854.